

# Explicit 2D Matrix Free Galerkin Finite Volume Solution of Plane Strain Structural Problems on Triangular Meshes

S.R. Sabbagh-Yazdi, N.E. Mastorakis, M. Esmaili

**Abstract**— In this paper, a novel matrix free Finite Volume Method based on Galerkin Approach is introduced for solution of weak form of two dimensional Cauchy equilibrium equations of plane strain solid state problems on linear triangular element meshes. The developed shape function free Galerkin Finite Volume structural solver explicitly computes stresses and displacements in Cartesian coordinate directions for the two dimensional solid mechanic problems under either static or dynamic loads. The accuracy of the introduced algorithm is demonstrated by comparison of computed results of two cantilever beams under static concentrated and uniformly distributed loads with analytical solutions. The performance of the solver is presented in terms of convergence behavior of the method. In order to present the applicability of the introduced method to solve dynamic problems, the computed displacements of a storage tank frame under oscillating hydrodynamic load is compared with the reported data in the literature.

**Key-Words**— Explicit Galerkin Finite Volume Method, Unstructured Linear Triangular Element, Computational Solid Mechanics

## I. INTRODUCTION

In the numerical analysis of the behavior of huge liquid-storage tanks, treatment of large-scale matrices becomes a burden owing to the hydrodynamic interaction between two different media, structure and liquid. In order to overcome such a problem, it is common to split the dynamic system into two separate problem regions [5]. Stresses and deformation of structural part of a storage tanks under seismic vibrations can be computed by replacing the effect of internal liquid by equivalent hydrodynamic load. Therefore, using empirical relations for estimation of distributed hydrodynamic load such as those proposed by Zanger and Westergard are one of the common techniques in dynamic fluid-structural interaction.

Over the last five decades a wide variety of numerical methods have been proposed for the numerical solution of

partial differential equations. Among them the Finite Element Method (FEM) has firmly established itself as the standard approach for problems in Computational Solid Mechanics (CSM), especially with regard to deformation problems involving non-linear material analysis [1,2].

It is well known that numerical analysis of solids in incompressible limit could lead to difficulties. For example, fully integrated displacement based lower-order finite elements suffer from volumetric locking, which usually accompanies pressure oscillation in incompressible limit [4]. Also there are some difficulties for producing stiffness matrix and shape function in order to increase the convergence rate.

Although certain restrictions on mesh configuration had to be imposed to avoid locking, these restrictions were less severe than those of the equivalent FEM meshes. Numerical calculation with meshes consisting of triangular cells showed excellent agreement with analytical results. Meshes consisting of quadrilateral FVM cells displayed too stiff behavior, indicating a locking phenomenon [4].

The FVM developed from early finite difference techniques and has similarly established itself within the field of computational fluid dynamics (CFD) [7,1]. However, similar to the FEM, the FVM integrates governing equation(s) over pre-defined control volumes [2], which are associated with the elements making up the domain of interest and therefore, preserve the conservation properties of the equations. Although, the Finite Volume Method (FVM) was originally developed for fluid flow and heat and mass transfer calculations [6], recently, it is generalized for stress analysis in isotropic linear and non-linear solid bodies. Therefore, the interest for FVM application to the structural analysis problems involving incompressible materials has grown during the recent years. From the results of several benchmark solutions, the FVM appeared to offer a number of advantages over equivalent finite element models. For instant it can be stated that, unlike the FDM solution, FVM solution is conservative and incompressibility is satisfied exactly for each discretised sub-domain (control volume) of the computational domain [4]. In principle, because of the local conservation properties the FVMs should be in a good position to solve such problems effectively.

Over the last decade a number of researchers have applied FVMs to problems in CSM [11] and it is now possible to classify these methods into two approaches, cell-centered and vertex-based ones. In this paper, the explicit approach introduced is based on Galerkin approach with a kind of

Manuscript received Sept. 2, 2007; Revised received January 18, 2008  
Saeed-Reza Sabbagh Yazdi, Associate Professor, of KNToosi University of Technology, Civil Engineering Department, No.1346 Valiasr Street, 19697-Tehran, IRAN [SYazdi@kntu.ac.ir](mailto:SYazdi@kntu.ac.ir) (Tel: 0098 21 88779473-5, Fax: 0098 21 88779476)

Mehdi Esmaili, Graduate Student, KN Toosi University of Technology, Civil Engineering Department, No.1346 Valiasr Street, 19697- Tehran, IRAN [Mehdiesma@gmail.com](mailto:Mehdiesma@gmail.com)

Nikos E. Mastorakis, Professor of Military Institutes of University Education (ASEI), Hellenic Naval Academy, Terma Chatzikyriakou 18539, Piraeus, GREECE [mastor@wseas.org](mailto:mastor@wseas.org)

matrix free vertex base FVM on meshes of linear triangular elements. The accuracy of the introduced method is assessed by comparison of computed stresses and displacements for two classical cantilever beams under static concentrated and uniformly distributed loads with analytical solutions and the performance of the solver is demonstrated in terms of convergence behavior of the method to the steady state condition. Then the structural frame of a storage tank under oscillating hydrodynamic pressure on its side walls, is performed by application of the introduced matrix free FVM and the computed results are compared with the data reported by the previous researchers [3].

## II. GOVERNING EQUATION

The universal law governing any continuum undergoing motion is given by general form of Cauchy's equilibrium equations:

$$\rho \ddot{u} = S^T \sigma + b \quad (1)$$

Where  $\sigma$  is the stress tensor,  $b$  is the body force,  $\rho$  is the material density and  $\ddot{u}$  is the acceleration.

For two dimensional problems,  $\bar{u} = (u_x, u_y)^T$  is the displacement vector and  $\sigma = (\sigma_{xx}, \sigma_{yy}, \sigma_{xy})^T$  is tensor vector. The operator  $S^T$  for two-dimensional problems is defined as,

$$S^T = \begin{bmatrix} \frac{\partial}{\partial x} & \circ & \frac{\partial}{\partial y} \\ \circ & \frac{\partial}{\partial y} & \frac{\partial}{\partial x} \end{bmatrix}$$

So, the matrix form of Cauchy equations for two-dimensional problems is:

$$\rho \begin{Bmatrix} \frac{\partial^2 u_x}{\partial t^2} \\ \frac{\partial^2 u_y}{\partial t^2} \end{Bmatrix} = \begin{bmatrix} \frac{\partial}{\partial x} & \circ & \frac{\partial}{\partial y} \\ \circ & \frac{\partial}{\partial y} & \frac{\partial}{\partial x} \end{bmatrix} \begin{Bmatrix} \sigma_{xx} \\ \sigma_{yy} \\ \sigma_{xy} \end{Bmatrix} + \begin{Bmatrix} b_x \\ b_y \end{Bmatrix} \quad (2)$$

For stress-strain relationship, the common Hook equation can be used as,

$$\sigma = D \varepsilon \quad (3)$$

Where  $D$  is the constitutive property matrix and for plane strain problems is:

$$D = \begin{bmatrix} I & \frac{\nu}{1-\nu} & \circ \\ \frac{\nu}{1-\nu} & I & \circ \\ \circ & \circ & \frac{1-2\nu}{2(1-\nu)} \end{bmatrix} \times \frac{E(1-\nu)}{(1+\nu)(1-2\nu)}$$

Here,  $\nu$  is the Poisson ratio and  $E$  is the Young modulus of elasticity. So the Cauchy's equilibrium equations in two Cartesian coordinate directions can be written as:

$$\begin{aligned} \rho \frac{\partial^2 u_x}{\partial t^2} &= \frac{\partial}{\partial x} \left( C_1 \frac{\partial u_x}{\partial x} + C_2 \frac{\partial u_y}{\partial y} \right) + \frac{\partial}{\partial y} C_3 \left( \frac{\partial u_x}{\partial y} + \frac{\partial u_y}{\partial x} \right) + b_x \\ \rho \frac{\partial^2 u_y}{\partial t^2} &= \frac{\partial}{\partial x} C_3 \left( \frac{\partial u_x}{\partial y} + \frac{\partial u_y}{\partial x} \right) + \frac{\partial}{\partial y} \left( C_2 \frac{\partial u_x}{\partial x} + C_1 \frac{\partial u_y}{\partial y} \right) + b_y \end{aligned} \quad (4)$$

Where for plane strain problems:

$$C_1 = \frac{E(1-\nu)}{(1+\nu)(1-2\nu)}, \quad C_2 = \frac{E\nu}{(1+\nu)(1-2\nu)}, \quad C_3 = \frac{E}{2(1+\nu)}$$

## III. DISCRETIZATION

In order to obtain the discrete form of the Cauchy's equation in  $i$  direction, the following form is used:

$$\rho \frac{\partial^2 u_i}{\partial t^2} = \frac{\partial \sigma_{ij}}{\partial x_i} + b_i \quad (j = 1, 2) \quad (5)$$

In which the stresses are defined as:

$$\begin{aligned} \sigma_{11} &= \left( C_1 \frac{\partial u_x}{\partial x} + C_2 \frac{\partial u_y}{\partial y} \right), \quad \sigma_{12} = C_3 \left( \frac{\partial u_x}{\partial y} + \frac{\partial u_y}{\partial x} \right) \\ \sigma_{21} &= C_3 \left( \frac{\partial u_x}{\partial y} + \frac{\partial u_y}{\partial x} \right), \quad \sigma_{22} = \left( C_2 \frac{\partial u_x}{\partial x} + C_1 \frac{\partial u_y}{\partial y} \right) \end{aligned}$$

By application of the Variational Method, after multiplying the residual of the above equation by the test function  $\omega$  and integrating over a sub-domain  $\Omega$  (Figure 1), in the absence of body forces we have,

$$\int_{\Omega} \omega \cdot \rho \frac{\partial^2 u_i}{\partial t^2} d\Omega = \int_{\Omega} \omega \cdot (\bar{\nabla} \cdot \bar{F}_i) d\Omega \quad (6)$$

Where,  $i$  direction stress vector is defined as  $\bar{F}_i = \sigma_{i1} \hat{i} + \sigma_{i2} \hat{j}$ .

The terms containing spatial derivatives can be integrated by part over the sub-domain  $\Omega$  and then equation 6 may be written as,

$$\int_{\Omega} \omega \rho \frac{\partial^2 u_i}{\partial t^2} d\Omega = [\omega \bar{F}_i]_{\gamma} - \int_{\Omega} (\bar{F}_i \cdot \bar{\nabla} \omega) d\Omega \quad (7)$$

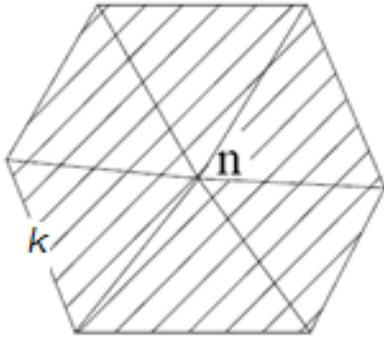


Fig.1 Sub-domain with area  $\Omega_n$

According to the Galerkin method, the weighting function  $\omega$  can be chosen equal to the interpolation function  $\phi$ . In finite element methods this function is systematically computed for desired element type and called the shape function. For a triangular type element (with three nodes), the linear shape functions,  $\phi_k$ , takes the value of unity at desired node  $n$ , and zero at other neighboring nodes  $k$  of each triangular element (Figure 2):

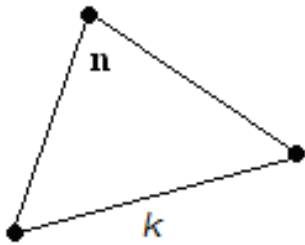


Fig.2. A linear triangular element

Therefore, the summation of the term  $[\omega \bar{F}_i]_{\gamma}$  over the boundary of the sub-domain  $\Omega_n$  is zero.

The right hand side (RHS) of the equation (7) can be discretized as:

$$\int_{\Omega} (\bar{F}_i \cdot \bar{\nabla} \phi) d\Omega \approx -\frac{1}{2} \sum_{k=1}^N (\tilde{F}_i \bar{\Delta l})_k \quad (8)$$

Where  $\bar{\Delta l}_k$  is normal vector of the side  $k$  opposite to the node  $n$  and  $\tilde{F}_i$  is the  $i$  direction piece wise constant stress vector at the centre of element associated with the boundary side  $k$  (inside the sub-domain  $\Omega_n$  with  $N$  boundary sides)

For a sub-domain formed by linear triangular elements sharing node  $n$ , the left hand side (LHS) of the equation (7) can be written in discrete form as:

$$\frac{\partial^2}{\partial t^2} \left( \int_{\Omega} \phi u_i d\Omega \right) \approx \frac{\Omega_n}{3} \frac{d^2 u_i}{dt^2} \quad (9)$$

A finite difference approach is applied for discretization of the time derivative of  $i$  direction displacement,  $u_i$ . Hence, the LHS of equation (7) can be written as,

$$\rho \frac{\Omega_n}{3} \frac{d^2 u_i}{dt^2} = \rho \left( \frac{u_i^{t+\Delta t} - 2u_i^t + u_i^{t-\Delta t}}{(\Delta t)^2} \right) \frac{\Omega_n}{3} \quad (10)$$

The final discrete form the equation (7) is obtained as,

$$\left( \frac{u_i^{t+\Delta t} - 2u_i^t + u_i^{t-\Delta t}}{(\Delta t)^2} \right) = \frac{3}{2\rho\Omega_n} \sum_{k=1}^N (\tilde{\sigma}_{i1} \Delta y - \tilde{\sigma}_{i2} \Delta x)_k \quad (11)$$

Considering direction  $i=1$  as  $x$  and  $i=2$  as  $y$ , the stresses  $\tilde{\sigma}_{i1}$ ,  $\tilde{\sigma}_{i2}$  are computed as,

$$\begin{aligned} \tilde{\sigma}_{xx} &= \left\{ C_1 \frac{\partial u_x}{\partial x} + C_2 \frac{\partial u_y}{\partial y} \right\} \approx \left\{ \frac{1}{A_k} \sum_{m=1}^3 (C_1 u_x \Delta y - C_2 u_y \Delta x) \right\}_m \\ \tilde{\sigma}_{xy} = \tilde{\sigma}_{yx} &= \left\{ C_3 \left( \frac{\partial u_x}{\partial y} + \frac{\partial u_y}{\partial x} \right) \right\} \approx \left\{ \frac{1}{A_k} \sum_{m=1}^3 (C_3 u_x \Delta y - C_3 u_y \Delta x) \right\}_m \\ \tilde{\sigma}_{yy} &= \left\{ C_2 \frac{\partial u_x}{\partial x} + C_1 \frac{\partial u_y}{\partial y} \right\} \approx \left\{ \frac{1}{A_k} \sum_{m=1}^3 (C_2 u_x \Delta y - C_1 u_y \Delta x) \right\}_m \end{aligned} \quad (12)$$

Where  $A_k$  is the area of triangular element (with  $m=3$  sides) associate with boundary side  $k$  of the sub-domain  $\Omega_n$  (Figure 3):

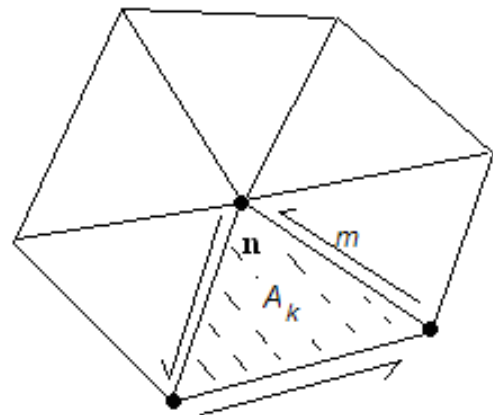


Fig.3: Triangular element with area  $A_k$  within the sub-domain  $\Omega_n$

#### IV. LOCAL TIME STEPPING

The time step  $\Delta t_n$  for each control volume can be computed as:

$$\Delta t_n \leq \frac{r_n}{c} \quad (13)$$

Where  $c$  is wave velocity. According to the wave velocity, gained by equation (14):

$$c = \sqrt{\frac{E}{\rho(1-\nu^2)}} \quad (14)$$

Here,  $r_n$  is the average radius of equivalent circle that matches with the desired control volume ( $r_n = \Omega_n / P_n$ ). For any control volume  $n$  this radius can be computed using area ( $r = \Omega_n / \sum_{k=1}^{N_{edge}} (\Delta I)_k$ ) and perimeter ( $P_n = \sum_{k=1}^{N_{edge}} (\Delta I)_k$ ) of the 2D control volume.

Due to the variations in sizes unstructured control volumes calculations, the allowable time step for computation of dynamic problems for the entire mesh is limited to the minimum associated with the smallest control volume of the domain. However, the large variation in grid size for the unstructured mesh will slow down the computations.

In present work, the local time step of each control volume is used for computation of static problems. In this technique to accelerate the convergence to steady state conditions, the computation of each control volume can advance using a pseudo time step which is calculated for its own control volume. The use of local time stepping greatly enhances the convergence rate.

V. INITIAL CONDITIONS

For static problems, an external load is considered as a global source term of Cauchy equations and is added to the LHS of described FVM formulation. Considering the linear shape function in each triangular cell, the value of the external load at the central node of the control volume is integrated over the control volume and considered at its central node. Fig.4 illustrates the area of the control volume which associates with the imposed load by considering the linear shape function in each triangular cell:

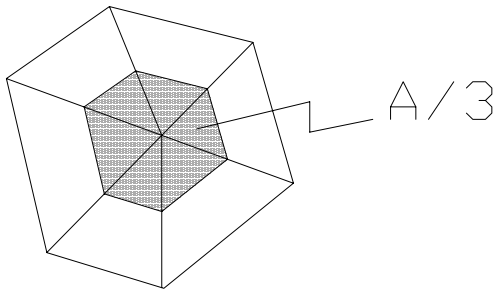


Fig.4 Imposing force area

But sudden imposing the external load would cause some

problems for the computational procedure. In order to overcome the problem, gradual load imposing is implemented in the present model using a relaxation coefficient which varies from 0.0 to 1.0 during some computational iteration.

$$Relaxation\ Coefficient = Min.\left\{\left(\frac{Istep}{L/\Delta t}\right), 1.\right\} \quad (15)$$

Where,  $Istep$  is the iteration number at desired stage of the computation,  $L$  is a length scale that can be assumed as the distance between maximum displacement and the centre of external load or constraint (support location).

For dynamic problems, the still initial condition is considered for the structure. However, for the storage tank case, firstly the hydrostatic condition is satisfied similar to the steady state problems. Then, the time dependent analysis would start.

VI. STATIC TEST CASES

The present structural solver is verified by two static test cases which are two cantilever beams under concentrated and distributed loads.

A. Cantilever Beam under Point Load

A standard problem in structural mechanics is that of a fixed-free cantilever supporting an applied load at the free end [9,1]. The fixed-free cantilever is shown in Fig.4. Here  $b=2.0$  is the breadth,  $L=20.0$  the length of the cantilever and  $F$  the applied load. It is assumed that the depth  $d=1.0$ . The static solution to this problem is available [9] and [8] as:

$$d_y = -\frac{4FL^3}{Edb^3} \quad (16)$$

Where,  $E$  is Young's modulus and  $d$  is the height of the cantilever beam.

Note that the gravity effect is not considered in this study. The static solution given by the above equation is independent of Poisson's ratio, Therefore, it is applicable to a cantilever undergoing pure flexure, i.e. no axial loads are supported and the out of plane load on the cantilever is zero. Thus for comparison with the analytic solution a zero Poisson's ratio is assumed.

The fixed-free cantilever is considered under a load of 200N at its free end, as depicted by Fig. 5.

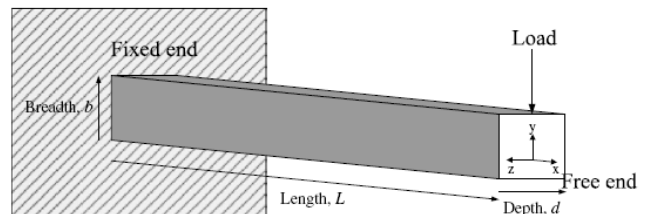


Fig. 5: Schematic of flexural deformation test of fixed-free cantilever

Table 1 Test case 1 cantilever beam specification

2D Fixed-free specification	value
Load, $F$	200 $N$
Length, $L$	20.0 $m$
Breadth, $b$	2.0 $m$
Density, $\rho$	2600.0 $kg/m^3$
Young's modulus, $E$	10 $MPa$
Poisson's ratio, $\nu$	0.0

With the parameters as given in Table 1, equation 16 gives the static displacement in  $y$  direction at the tip of the cantilever as 0.08 m.

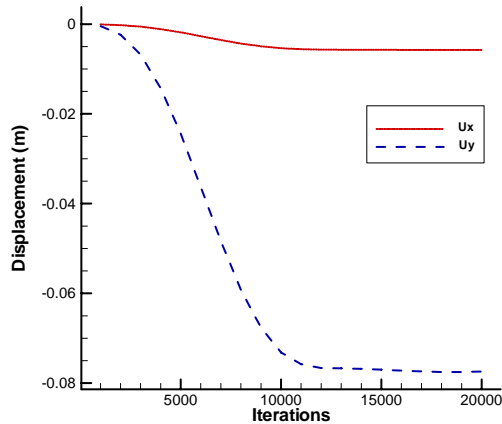


Fig.6. Converged results for tip displacements (80\*8 mesh)

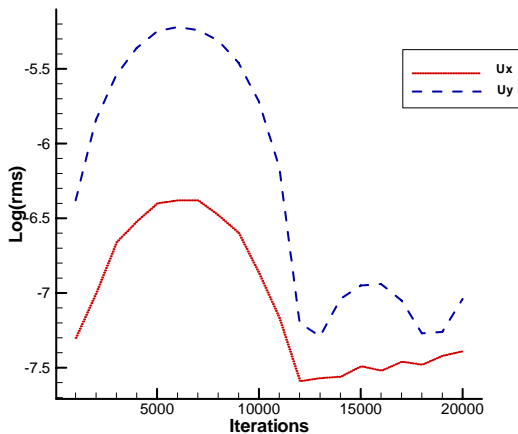


Fig.7. Convergence of the logarithm of root mean square of the displacements (80\*8 mesh)

In order to provide a better understanding about the effects of gradual load imposing technique, the convergence behavior of the computed displacements are shown in Fig.6 and the root mean square of the computed displacements are shown in Fig.7. As can be seen the logarithm of root mean square errors of displacements increase by gradual activation of the load in the initial stages of the computation. Then the logarithm of root mean square errors computed displacements present a decrease up to 7 orders of magnitude when the load is fully

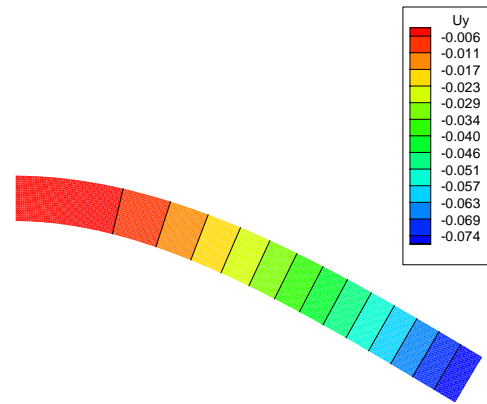
imposed.

The error percentages for the numerical solutions of the problem on various meshes \*(with various grid spacing sizes) are tabulated in table 2.

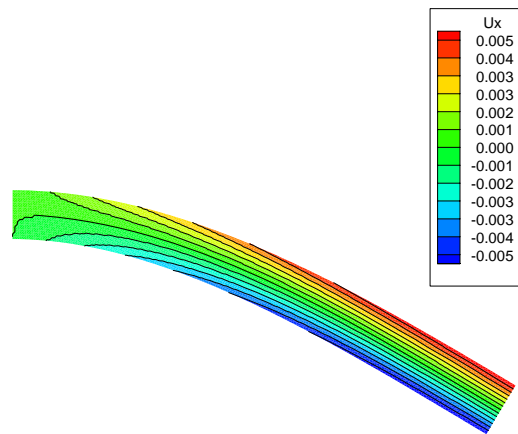
Table 2.Cantilever beam error report

Elements	Vertical displacement at free end	Error for computed values
20*2 triangular	-0.05968	25.4%
40*4 triangular	-0.072169	9.78%
80*8 triangular	-0.077522	3.09%
100*10 triangular	-0.0786	1.7%
200*20 triangular	-0.08007	0.08%

Computed displacements and stresses contours are illustrated in following figures (Fig.8 and Fig.9).

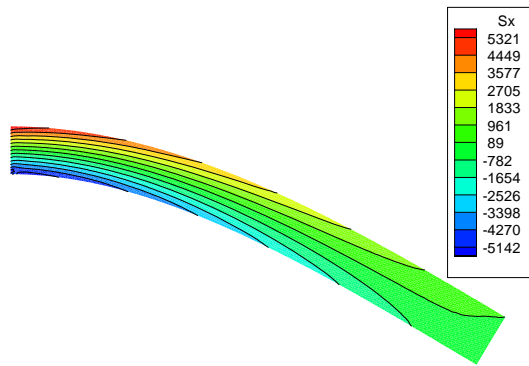


a) vertical displacement contours

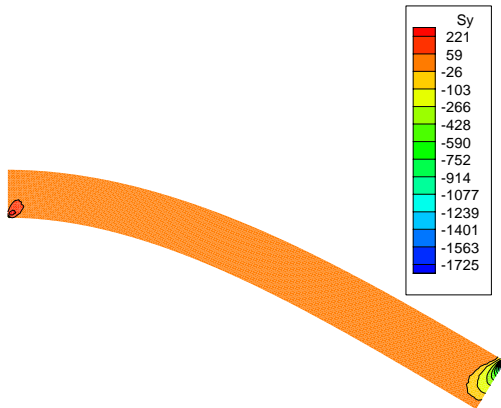


b) horizontal displacement contours

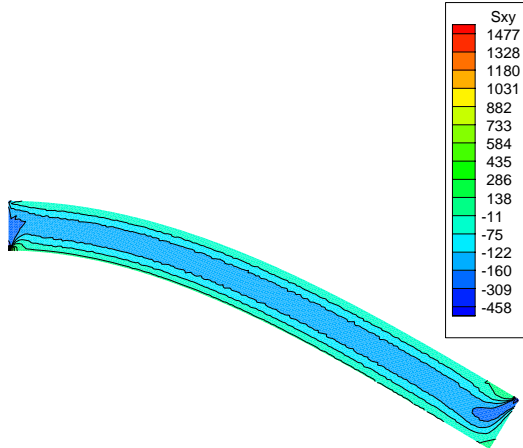
Fig.8 Color coded maps of computed displacements



a)  $\sigma_{xx}$  stress contours



b)  $\sigma_{yy}$  stress contours



c)  $\sigma_{xy}$  stress contours

Fig.9 Color coded maps of computed stresses

**B. Cantilever Beam under Uniform Distributed Load**

The two dimensional cantilever, shown in Fig. 10, is considered under uniform load. Wall specifications are shown in Table.3 with  $100 \text{ N/m}$  uniform load.

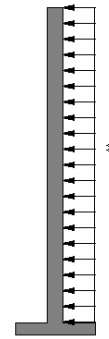


Fig.10. Cantilever under uniform distributed load

The displacement of wall's tip computed by following equation [10]:

$$d_x = \frac{wL^4}{8EI} \tag{17}$$

Analytical solution using the above equation shows  $0.03m$  displacement on tip and by application of the present Galerkin finite volume method (GFVM) structural solver  $0.0301m$  horizontal displacement is computed using a  $200 \times 20$  triangular mesh. Computed results present  $0.33\%$  error in  $x$  direction displacement. Some samples of computed stress contours are plotted in Fig.11.

Table 3. Wall Specification

2D Wall specification	value
Load, $W$	$100 \text{ N}$
Length, $L$	$2.0 \text{ m}$
Breadth, $b$	$0.2 \text{ m}$
Density, $\rho$	$2600.0 \text{ kg/m}^3$
Young's modulus, $E$	$10 \text{ MPa}$
Poisson's ratio, $\nu$	$0.0$

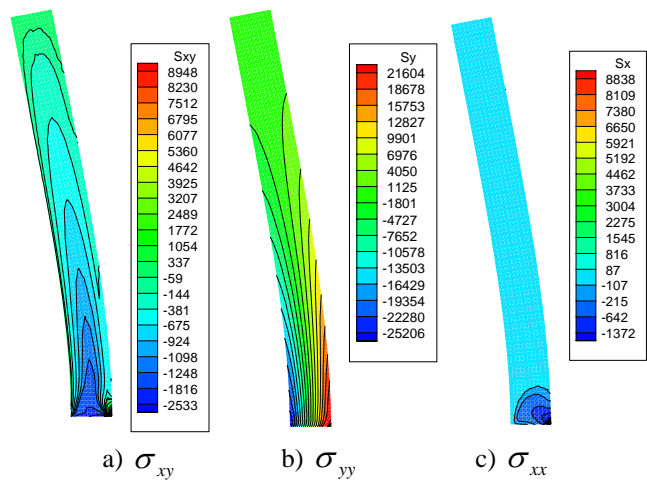


Fig.11. Stress contours on the wall

VII. DYNAMIC TEST CASE

A rectangular storage tank, oscillated with seismic loads, is

utilized for investigation of introduced method performance in solution of dynamic problems. The storage tank under oscillating load, for which experimental measurements are available [3], is shown in Fig.12 and its specifications are presented in Table 4.

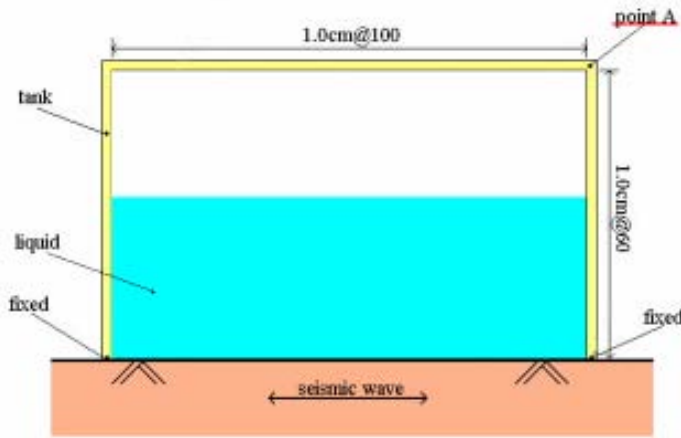


Fig.12. Oscillating tank

Table 4. Storage tank structure specifications[3].

Parameters	Value
Young's modulus, $E$	21 MPa
Density, $\rho$	$7850 \left( \frac{kg}{m^3} \right)$
Poisson ratio, $\nu$	0.3
Area	$0.05 m^2$

It is assumed that the water volume is conserved in the tank. Therefore, the increase in water level on the right vertical side wall is followed by decrease in water level of the other side water. As a function of water level, the opposite directions hydrostatic and hydrodynamic distributions of the horizontal pressure loads are imposed on both walls at each incremental the time of oscillation. Sloshing and free surface waves effects are assumed to be negligible. So, the Zanegar [12] and Westergard [13] global relations for the hydrodynamic load distributions are applied. An unstructured mesh with 1633 nodes and 2592 triangular elements applied to simulate the storage tank structure behavior during the oscillation time (Fig.13).



Fig.13. unstructured mesh applied for GFVM solver

In order to impose the fixed boundary conditions, zero displacements are imposed at lower boundaries of the mesh. After computation of stresses and deformation under hydrostatic load using local time stepping, the time dependent (dynamic) computations are performed using global minimum time step of the domain.

In figure 14, the time history of deformations of top right wall (point A in Fig. 12) computed by imposing hydrostatic and two hydrodynamic load distributions are compared with the reported experimental measurements. As can be seen the computed results presents good agreements with experimental measurements.

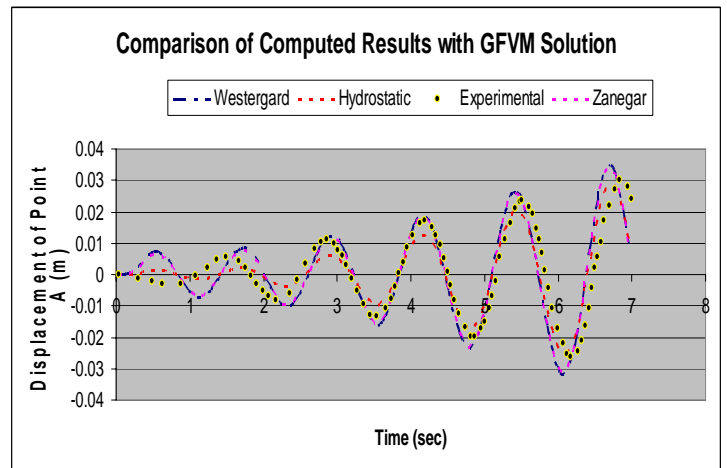


Fig.14. Horizontal deformation of point A

The computed stress contours at  $t=6.97$  (s) are demonstrated in the following figures (Fig. 15).

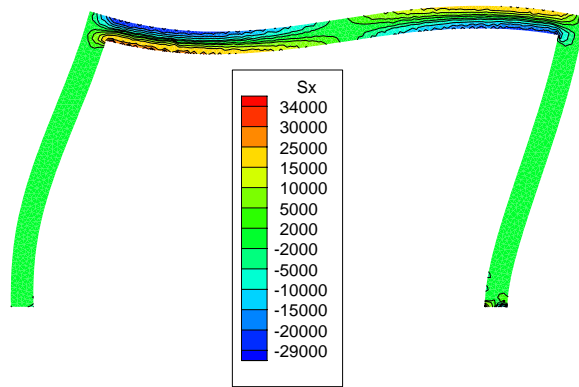
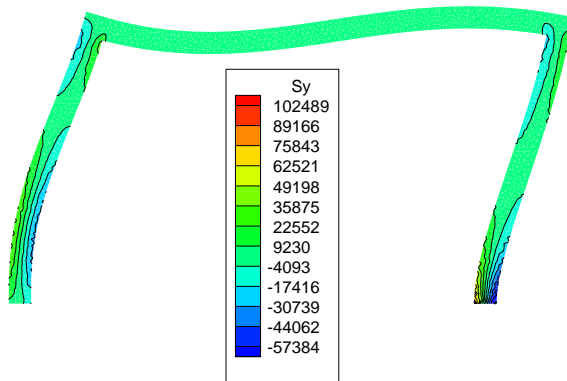
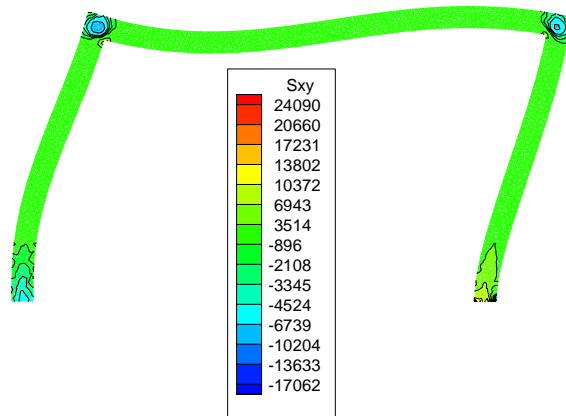
a)  $\sigma_{xx}$  stress contoursb).  $\sigma_{yy}$  contoursc).  $\sigma_{xy}$  contours

Fig.14 : Computed results for oscillating storage tank

### VIII. CONCLUSION

A vertex base Galerkin Finite Volume method for explicit matrix free solution of two dimensional Cauchy equations is introduced in this paper. This computational model solves stress and deformation of solid mechanics under static and dynamic loads. The performance of described the computational solid mechanic algorithm is examined for various size of the meshes for a cantilever beam under a point load. Since there is no interpolation function in the numerical formulation of the present solver, the fine meshes provide

more accurate results than the coarse meshes.

The present model is examined for some plane strain structural problems. After verification of the model for static concentrated and uniformly distributed loads on two cantilever beams, it is applied for solution of stresses and deformations an oscillating storage tank frame under hydrodynamic loads estimated by two empirical relations. The comparison of the computed results of static and dynamic problems with analytical solution and experimental measurements presents promising agreements.

The new explicit matrix and shape function free numerical method with light computational work load can easily be extended to three dimensions and be applied for solving large deformations of real world solid mechanics problems with complicated geometries.

### References

- [1] X. Lv, Y. Zhao, X.Y. Huang, G.H. Xia, X.H. Su, "A matrix-free implicit unstructured multigrid finite volume method for simulating structural dynamics and fluid-structure interaction", *Journal of Computational Physics*, 2007 (to be appeared)
- [2] O.C. Zienkiewicz, R.L. Taylor, "*The Finite Element Method Basic Formulation and Linear Problems*", Vol.1, McGraw-Hill, Maidenhead, UK, 1989.
- [3] H. Ogawa, "An analysis of interaction problem between sloshing and structure", *Chuo Univ., Kasuga 1-13-27*
- [4] I. Bijelonja, I. Demirdžić, S. Muzaferija, "A finite volume method for incompressible linear elasticity" *Journal of Mechanical Engineering*. 195, 2006, pp 6378-6390
- [5] J. R. Cho, J.-M. Song, "Assessment of classical numerical models for the separate fluid-structure modal analysis", *Journal of Sound and vibration* 239(5), 2001, pp. 995-1012
- [6] I. Demirdžic, D. Martinovic, "Finite volume method for thermo-elasto-plastic stress analysis", *Computer Methods in Applied Mechanics and Engineering* 109, 199, pp. 331-349.
- [7] C. Bailey, G.A. Taylor, M. Cross, P. Chow, "Discretisation procedures for multi-physics phenomena", *Journal of Computational and Applied Mathematics* 103, 1999, pp. 3-17
- [8] R.T. Fenner, *Engineering Elasticity: Applications of Numerical and Analytical Techniques*, Ellis Horwood, 1986.
- [9] S.P. Timoshenko, J.N. Goodier, *Theory of Elasticity*, McGraw-Hill, New York, 1982.
- [10] F.P. Beer & E. R. Johnston, "*Mechanics of Materials*", JR. McGraw-Hill, 1992.
- [11] A.K. Slone, C. Bailey, M. Cross, "Dynamic solid mechanics using finite volume methods", Old Royal Naval College, University of Greenwich, Applied Mathematical Modeling 27, 2003, pp 69-87
- [12] "*Design of Small Dams*", United States Department of The Interior, third edition 1987
- [13] H. M. Westergaard, "*Water Pressures on Dams During Earthquakes*", Meeting of ASCE, 1932

First Author's biography may be found in:

<http://sahand.kntu.ac.ir/~syazdi/>

Second Authors' biography may be found in: <http://www.wseas.org/mastorakis>